An Investigation of Weld Hot Cracking in Duplex Stainless Steels

Cracking susceptibility in commercial grades is linked to a Cu- and P-enriched, low-melting liquid film

BY D. E. NELSON, W. A. BAESLACK III AND J. C. LIPPOLD

ABSTRACT. The weld fusion zone hot cracking behavior of four duplex stainless steel alloys was investigated using the Varestraint test. The duplex stainless steels evaluated included: Ferralium Alloy 255 (UNS-S32550), Uddeholm NU744LN (UNS-S31803), and two experimental Fe-Cr-Ni alloys. Two commercial Type 304L alloys were included in the study for comparison.

Varestraint test results indicated that the commercial duplex stainless steels were more susceptible to fusion zone hot cracking than the experimental alloys and a Type 304L alloy which exhibited Ferrite Number (FN) 4.5 in the weld fusion zone. All of the duplex alloys were less susceptible to hot cracking than the Type 304L alloy, which solidified as austenite and exhibited a ferrite-free fusion zone microstructure.

Metallographic inspection of Varestraint specimens revealed that fusion zone hot cracking in the duplex alloys was associated with grain boundaries which had been fully ferritic during the final stages of solidification. Microprobe analysis of the remnants of liquid films along the crack paths in the commercial alloys revealed increased levels of copper, molybdenum, nickel and phosphorus. It is suggested that the partitioning of copper and phosphorus to the ferritic solidification boundaries promoted the formation of complex low-melting liquid films which readily wet the single-phase boundaries. The lower hot cracking susceptibility of the experimental duplex alloys appears to be due to the absence of these complex synergistic alloying element effects.

Fractographic study of the hot crack surfaces in the duplex alloys showed both dendritic and flat columnar topographies. The flat regions, which were found at locations on the fracture surface farthest from the crack front at the time of straining, have been attributed to grain boundary formation and migration during and immediately subsequent to the final stages of fusion zone solidification. It is postulated that the incidence of flat fracture is related to the greater susceptibility of the duplex alloys to weld solidification cracking versus the FN 4.5 Type 304L alloy, which exhibited an exclusively dendritic surface.

D. E. NELSON is with Hughes Aircraft Co., El Segundo, Calif. W. A. BAESLACK III is with the Department of Welding Engineering, Ohio State University, Columbus, Ohio. J. C. LIPPOLD is with the Edison Welding Institute, Columbus, Ohio.

Based on a paper presented at the 66th Annual AWS Meeting, held April 28 to May 3, 1985, in Las Vegas, Nev.

Introduction and Background

The duplex stainless steels have been developed to provide a higher strength, corrosion-resistant alternative to the 300-series austenitic stainless steels. Relative to the conventional Type 304L and 316L alloys, the duplex stainless steels typically contain increased chromium (22–26 wt-%), decreased nickel (4–8 wt-%), increased molybdenum (2–5 wt-%), increased nitrogen (0.1–0.2 wt-%), and occasional additions of copper. These alloy modifications impart excellent resistance to pitting, crevice corrosion, and stress-corrosion cracking (Refs. 1–4). The increase in ferrite-stabilizing elements (Cr, Mo) relative to austenite-stabilizing elements (Ni, N) in these alloys results in a microstructure which is "duplex" in nature, containing both ferrite and austenite. Duplex stainless steel base materials are normally solution heat treated at a temperature which produces nearly equal proportions of ferrite and austenite.

KEY WORDS

Duplex Stainless Stl
Weld Hot Cracking
Crack Susceptibility
Zone Solidification
Element Segregation
Varestraint Testing
Alloy UNS-S32550
Alloy UNS-S31803
Fe-Cr-Ni Alloys
Microprobe Analysis

The unique properties of the duplex stainless steels have resulted in their use in a variety of industrial applications, including chemical process plant piping, oil and gas transmission lines, and structures for use in marine environments (Refs. 5, 6). Since welding is widely used in the fabrication of many components used in these applications, understanding the factors which affect the weldability of duplex stainless steels is critical to the successful implementation of these engineering materials.

Weld Hot Cracking

Weld hot cracking, or solidification cracking, generally occurs slightly above the melting temperature of the lowest melting constituent, sometimes referred to as the effective solidus temperature (Refs. 7, 8). At this point in the weld solidification process, adjacent dendrites have impinged upon each other to form solidified bridges, which are surrounded by regions containing lower-melting interdendritic liquid. These solid bridges are subject to the greatest proportion of shrinkage-induced strain as the surrounding material cools. A threshold amount of either low-melting liquid or strain may cause fracture of these solid bridges and the subsequent formation of a weld hot crack (Refs. 9–12). By definition, weld hot cracks are interdendritic in nature, occurring either between individual dendrites or, more commonly, along a weld "grain boundary," where dendrites of different

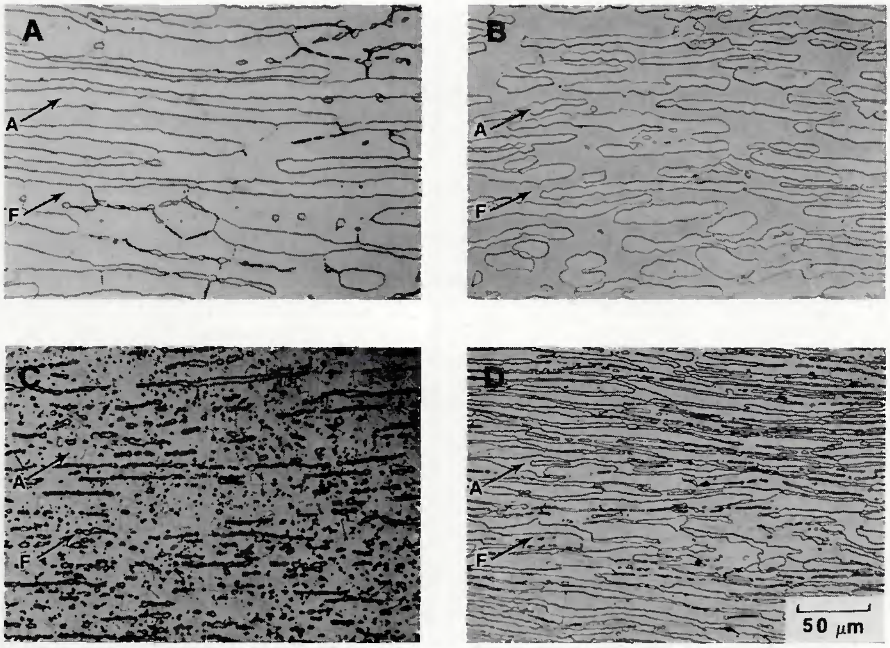

Fig. 1—Base metal microstructures of the duplex stainless steels. A—Ferralium Alloy 255; B—Uddeholm NU744LN; C—Alloy 21-9; D—Alloy 23-7. The ferrite (F) and austenite (A) phases are indicated

growth orientation impinge. The threshold level of both strain and interdendritic liquid necessary to cause cracking is material specific and depends to a large extent on both the composition of the material and the welding conditions.

Austenitic Stainless Steels

Weld hot cracking of the austenitic stainless steels has been the subject of considerable research interest over the past 30 years. The beneficial effect of delta ferrite was first recognized in the 1940's and has since been substantiated by many investigators (Refs. 13–24). Early studies by Borland (Ref. 14) and Hull (Ref. 15) demonstrated that austenitic stainless steel welds and castings which contained between 5 and 10 vol-% delta ferrite provided optimum resistance to hot cracking in a variety of alloy systems. Since these initial observations, additional studies have investigated the metallurgical basis accounting for the beneficial effect of weld metal ferrite. Masumoto, *et al.* (Ref. 17), first reported the influence of solidification behavior on cracking susceptibility. They found that alloys whose primary solidification product was ferrite were much more resistant to hot cracking than alloys whose primary solidification product was austenite. The presence of at least 5 vol-% ferrite in the as-welded microstructure was merely an indication that weld solidification occurred as primary ferrite. Austenitic stainless steel welds which were either fully austenitic or contained only a small amount of ferrite (< 2 vol-%) generally solidified as primary austenite and were susceptible to hot cracking (Refs. 18, 20, 22–26).

Duplex Stainless Steels

Weld hot cracking in the duplex stainless steels has received considerably less attention. These alloys solidify as ferrite and may exhibit from 20 to 80 vol-% ferrite in the as-welded microstructure. Based on the correlation between cracking susceptibility and solidification behavior developed for the austenitic stainless steels, the susceptibility of the duplex alloys to hot cracking would be expected to be low.

In fact, Hull (Ref. 15) reported that hot cracking in small cast ingots of austenitic stainless steels increased as the ferrite content of the as-solidified ingot increased above 10 vol-%. He proposed that the optimum cracking resistance of the castings containing 5 to 10% ferrite resulted from the presence of significant austenite-ferrite interfacial area during the final stages of solidification. The low interfacial energy of these two-phase boundaries inhibits boundary wetting by low-melting liquid films, thus reducing the propensity for separation (cracking) along these boundaries. He further postulated that like-phase boundaries, such as austenite-austenite or ferrite-ferrite grain or subgrain boundaries, would be more susceptible to cracking due to more extensive wetting by liquid films.

Suutala, *et al.* (Refs. 20, 26, 27), observed that the cracking susceptibility in a wide range of stainless steels could be correlated with a Cr_{eq}/Ni_{eq} ratio. At low ratio values, primary solidification occurred as austenite and cracking susceptibility was high. Above a threshold value of Cr_{eq}/Ni_{eq}, primary solidification shifted to ferrite and cracking propensity decreased. A further increase in this ratio, which resulted in welds containing more than 30 vol-% ferrite, again resulted in an increase in cracking. Suutala, *et al.* (Refs. 20, 26, 27), suggested that this increase in cracking results from a shift in solidification behavior during the final stages of freezing. Below approximately 30 vol-% ferrite, some austenite forms at the interstices of the primary ferrite dendrites as a secondary solidification product. The presence of austenite during the final stages of solidification inhibits interdendritic wetting and reduces crack susceptibility, as proposed by Hull (Ref. 15). In welds which exhibit more than 30 vol-% ferrite, solidification is entirely ferritic, and interdendritic liquid films are more likely to wet the ferrite-ferrite boundaries.

Despite the metallurgical rationale which suggests increased hot cracking susceptibility of the duplex stainless steels relative to austenitic stainless steels, only a few instances of weld hot cracking in these materials have been reported (Refs. 28–30). Gooch (Ref. 29) observed cracking only when welding plate thicknesses were above 10 mm (0.4 in.). Blumfield, *et al.* (Ref. 28), and Flasche (Ref. 30) have reported only minor difficulties with hot cracking in Ferralium Alloy 255. The apparent discrepancy in hot cracking behavior predicted by laboratory results and that actually encountered during field fabrication is puzzling in light of the good correlation obtained with the austenitic stainless steels.

This investigation was designed to evaluate the relative hot cracking susceptibility of four duplex and two austenitic stainless steel alloys and relate the observed hot cracking behavior to the solidification behavior of the individual alloys.

Material and Experimental Procedure

Materials

The duplex stainless steels which were studied included: Ferralium Alloy 255 (UNS-S32550), a nitrogen-bearing steel with approximately 26Cr-5Ni-2Cu-3.3Mo; Uddeholm NU744LN (UNS-S31803), a nitrogen-bearing steel containing approximately 22Cr-6Ni-3Mo; and two experimental alloys, designated as 21-9 and 23-7, which were simple alloys of the Fe-Cr-Ni system, containing approximately 21Cr-9Ni-2Mn and 23Cr-7Ni-2Mn, respectively. All material was in the form of plate which had been solution-annealed at 1020°–1100°C (1870°–2010°F), followed by rapid cooling in air or water.

The as-received base metal microstructures for the four duplex stainless steel alloys studied are illustrated in Fig. 1. Ferralium Alloy 255, Uddeholm NU744LN

Table 1—Compositions for the Alloys Investigated (wt-%)

Materials	Cr	Ni	Si	Mn	Mo	Cu	C	N	S	P
Ferralium Alloy 255	24.9	5.4	0.54	1.1	3.1	1.7	0.027	0.17	0.001	0.023
Uddeholm NU744LN	21.6	4.9	0.44	1.7	2.4	0.2	0.067	0.10	0.001	0.024
Alloy 21-9	20.8	9.0	0.62	1.7	0.07	–	0.024	0.007	0.008	0.025
Alloy 23-7	22.8	7.1	0.54	1.8	0.06	–	0.033	0.006	0.009	0.027
304L (FN 0)	18.3	11.4	0.41	1.7	0.04	–	0.023	0.037	0.002	0.007
304L (FN 4.5)	18.6	10.7	0.54	1.9	0.21	–	0.017	0.040	0.001	0.024

Table 2—Mini-Varestraint Test Parameters

Current	180 ± 10 A
Voltage	17 ± 1 V
Travel speed	152 mm/min (6 ipm)
Electrode-to-work distance	2.38 mm (3/32 in.)
Electrode	$W.ThO_2$, 60-deg included angle
Electrode diameter	2.38 mm (3/32 in.)
Ram velocity	300 mm/s (11.7 in./s)
Shielding gas	Argon
Flow rate (Torch)	0.29 L/s (40 cfh)
Flow rate (Trail)	0.53 L/s (70 cfh)

and the 23-9 alloy all exhibited approximately equal proportions of austenite and ferrite, while the 21-9 alloy contained a greater proportion of austenite. Also evident from Fig. 1 is the elongated morphology of the ferrite. The austenite phase, which formed at ferrite-ferrite grain boundaries, was also elongated, with the exception of the 21-9 alloy, in which an equiaxed austenite grain structure was observed.

A conventional Type 304L stainless steel which contained approximately 5 vol-% (FN 4.5) delta ferrite in the weld fusion zone at room temperature and a Type 304L stainless steel which remained fully austenitic in the weld fusion zone were also tested in order to provide a baseline for comparison of the hot cracking susceptibilities of the duplex stainless steels. Complete compositional analyses for all the alloys tested are shown in Table 1.

Varestraint Testing

The mini-Varestraint test (Ref. 31) was utilized to assess the relative weld hot cracking susceptibility of the duplex and austenitic alloys. As-received 12.8-mm (0.5-in.) thick plates were machined into test specimens with dimensions of 0.64 × 2.54 × 15.24 cm (0.25 × 1.0 × 6.0 in.). The specimens were thoroughly degreased with acetone and wiped dry immediately prior to testing. The GTA welding parameters used in mini-Varestraint testing are listed in Table 2.

The specimens were tested over a range of augmented strains from 0.5 to 5%. The augmented strain, ξ, is given by the following equation:

$$\xi \approx t/2R$$

where t is the specimen thickness and R is the radius of the die block over which the specimen is deformed.

Following testing, the specimens were chemically cleaned using an alkaline permanganate-citrate acid method (Ref. 32) to remove high-temperature oxides which made observation of hot cracks difficult. The samples were first immersed for 1 h in a boiling solution containing 10% NaOH and 3% $KMnO_4$ in 1 L of water. After rinsing in water, the samples were immersed for 1 h in a boiling solution containing 12 g ammonium citrate, 100 mg EDTA, and 1 L of water, in which the pH was adjusted to 4–4.5 with citric acid. This cleaning method effectively removed the oxide without attacking the underlying metal. A quantitative measure of the extent of hot cracking in each sample was determined using a binocular microscope equipped with a filar eyepiece. The number and length of all cracks produced along the trailing edge of the weld pool during the mini-Varestraint test were determined at 70X magnification.

Metallography

Selected mini-Varestraint test specimens were sectioned, mounted, and polished with 0.05 micron alumina for metallographic analysis. Sections were made through the cracked regions of the test specimens to reveal the hot crack morphology and in unstrained areas for a more detailed examination of the weld fusion and heat-affected zone structures. Samples were etched using either a mixed acid reagent containing equal amounts of nitric, hydrochloric, and acetic acid or a 10% oxalic acid electrolytic etch at 6 V for 10–20 s.

Fractography

Selected Ferralium Alloy 255 and Uddeholm NU744LN test samples containing hot cracks were carefully sectioned and broken in order to reveal hot crack fracture surfaces. The fracture surfaces were examined using a scanning electron microscope (SEM) equipped with an energy dispersive spectrometer (EDS) in order to characterize the fracture morphology and identify particles or phases which were associated with the hot crack surface.

Analytical Evaluation

An electron microprobe was used to determine the degree of solute segregation associated with solidification and hot cracking in the commercial duplex alloys. The analyses were performed at an accelerating voltage of 25 kV and a beam current of 10 nA, producing an effective probe size of approximately 1 μm (0.00004 in.).

Hot crack surface analysis was also performed on the commercial alloys, using a scanning Auger microprobe (SAM). An accelerating voltage of 5 kV and a beam current of 1.85 μA were used to examine the surface. Composition depth profiles were obtained to a depth of 100 nm by sputtering the surface with a beam of argon ions.

Results

Predicted Solidification and Transformation Behavior

The solidification and solid-state phase transformation behavior of austenitic and duplex stainless steels is a strong function of the composition of the particular steel. Since the duplex stainless steels are basically high-Cr, low-Ni versions of the austenitic stainless steels, the Fe-Cr-Ni ternary system is useful for predicting the solidification and solid-state transformation characteristics of these materials. The pseudo-binary section of the Fe-Cr-Ni ternary system at 60 wt-% iron (Ref. 33), shown in Fig. 2, can be used to describe the behavior of a typical duplex stainless steel upon cooling from the solidification range. A nominal composition, C_o, at 30Cr-10Ni, has been selected as representative, since the majority of commercial alloys contain molybdenum and nitrogen additions which increase their "effective" chromium and nickel contents (Cr- and Ni-equivalents), respectively.

Alloys which lie to the right of the triangular, three-phase region at approximately 25Cr-15Ni in Fig. 2 solidify as primary ferrite. Alloys which solidify as ferrite in close proximity to this three-phase region may form some austenite during the final stages of solidification, as a consequence of a peritectic/eutectic reaction (Refs. 21, 23). As the composition is enriched in chromium and depleted in nickel at a constant iron content, this reaction becomes less favorable and solidification is completely ferritic. Thus, Fig. 2 predicts that duplex stainless steels will solidify as primary ferrite with little or no austenite forming as a secondary solidification product.

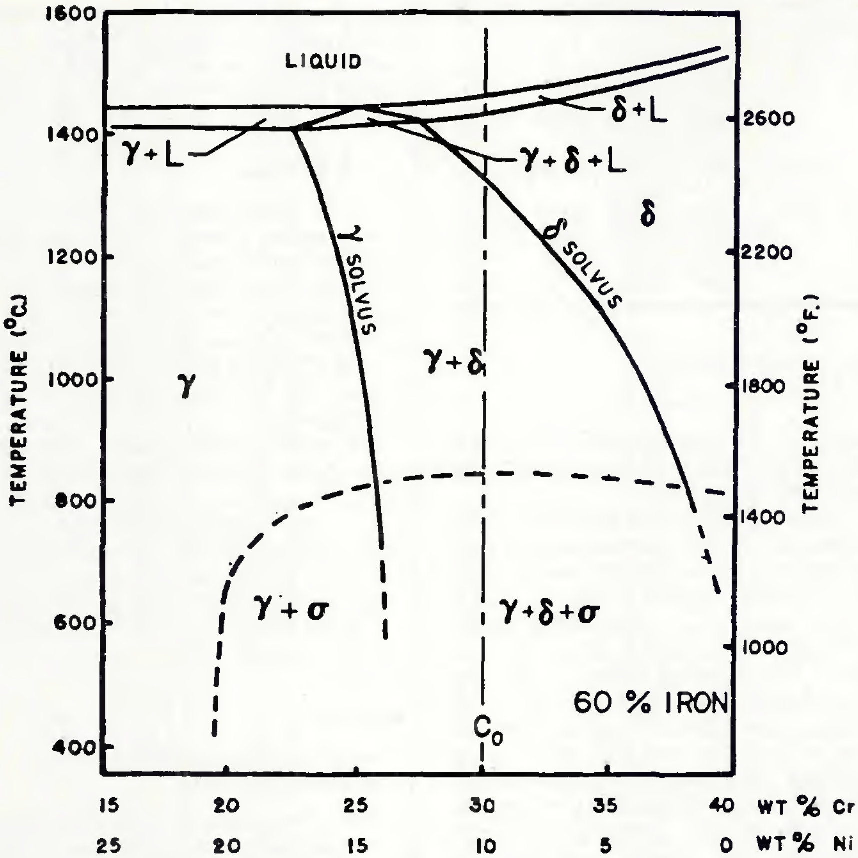

Fig. 2 — Vertical section of the Fe-Cr-Ni phase diagram at 60% iron. The C_o composition line represents a typical duplex stainless steel (Ref. 32)

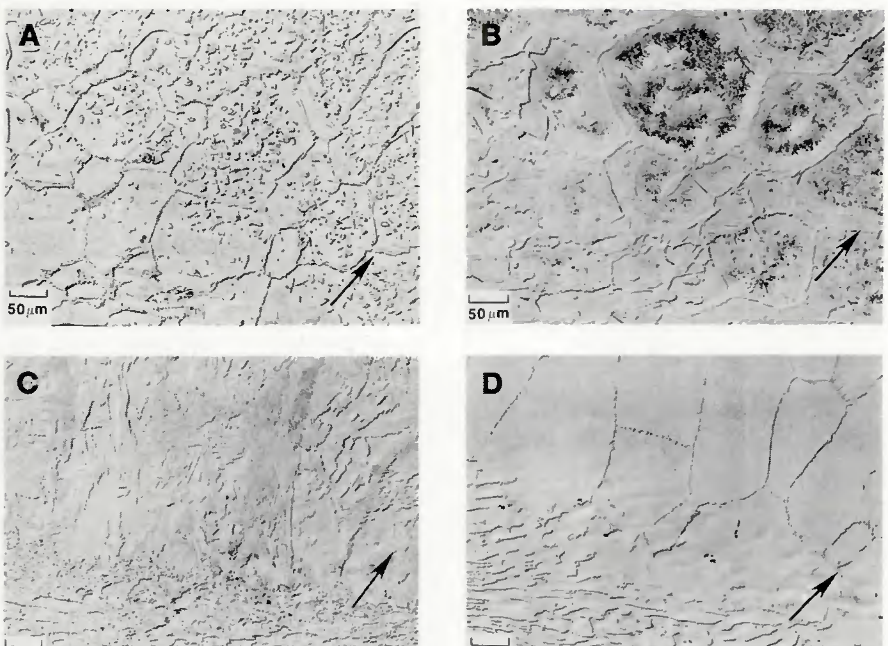

Fig. 3 — The weld fusion boundary regions of the duplex stainless steels evaluated. A — Ferralium Alloy 255; B — Uddeholm NU744LN; C — Alloy 21-9; D — Alloy 23-7. Arrows indicate the approximate location of the weld fusion interface

Following solidification, a duplex stainless steel of composition C_0 enters the single-phase ferrite region of the phase diagram. Within this region, diffusion is rapid, and much of the elemental partitioning resulting from solidification may be reduced, depending primarily on the rate of cooling through this region. Upon further cooling, the alloy enters the austenite plus ferrite phase field and a gradual transformation of ferrite to austenite occurs. The austenite will form preferentially at defect structures in the ferrite, *e.g.*, grain and solidification substructure boundaries, which may be enriched in elements which stabilize austenite (Ni, Mn, Cu, N, C). Note that, unlike the austenitic stainless steels, a typical duplex stainless steel remains within the bounds of the austenite plus ferrite region to room temperature. As a result, the fusion zone of these alloys would be expected to contain a large fraction of ferrite in the room-temperature microstructure.

The pseudo-binary diagram in Fig. 2 can also be used to explain the effect of the solution-annealing temperature on the microstructure and phase composition of the duplex stainless steel base materials. Solution annealing an alloy of composition C_0 in the temperature range from 1020° to 1100°C results in an equilibrium mixture containing nearly equal proportions of ferrite and austenite. The composition of these phases would be roughly approximated by the austenite and ferrite solvus lines at the solution-annealing temperature. Since the width of the two-phase region is large, a significant difference in composition should exist between the ferrite and the austenite. (This assumes that the alloy is held at the solution-annealing temperature long enough to achieve equilibrium and that the isothermal tie line lies in the plane of the 60% iron section.)

Weld Microstructures

The weld fusion zone and fusion boundary region microstructures of the duplex stainless steels evaluated during this investigation are shown in Fig. 3. These microstructures are representative of welds made using the parameters listed in Table 2. The fusion zone microstructure of Ferralium Alloy 255 (Fig. 3A) consists of large, epitaxial ferrite grains with continuous austenite networks at prior ferrite grain boundaries and intragranular austenite precipitates. The weld ferrite content of the Ferralium Alloy 255, determined using the Extended Ferrite Number (EFN) scale of the Magne-Gage (Ref. 34), was on the order of EFN 60. The adjacent heat-affected zone (HAZ) also exhibited a continuous grain boundary austenite network but showed little intragranular austenite precipitation. Instead, a fine precipitate was observed to be localized in the ferrite phase. These particles could not be precisely identified, but were found to be enriched in chromium (Ref. 35). A precipitate-free zone corresponds to regions surrounding the austenite, suggesting that austenite may act as a sink for fast-diffusing, interstitial elements, such as carbon and nitrogen, which may be integral in the formation of the precipitate.

The weld microstructure and fusion boundary region of the Uddeholm NU744LN steel are shown in Fig. 3B. The ferrite content of the fusion zone was approximately EFN 70. Similar to the Ferralium Alloy 255, continuous austenite networks existed at the ferrite grain boundaries. A fine distribution of intragranular precipitates was observed within the fusion zone, reminiscent of the HAZ microstructure in the Ferralium Alloy 255 (Fig. 3A).

The weld structure of Alloy 21-9, shown in Fig. 3C, consisted of large ferrite grains with Widmanstatten-type austenite precipitating from the grain boundary austenite. The ferrite content of the Alloy 21-9 fusion zone was on the order of EFN 40, the lowest of the four duplex alloys evaluated. Alloy 23-7 exhibited a highly ferritic fusion zone microstructure with a ferrite content of approximately EFN 80 (Fig. 3D). Austenite in the Alloy 23-7 fusion zone was restricted almost exclusively to the grain boundaries. The fine intragranular precipitation observed in the Uddeholm NU744LN fusion zone was not apparent in Alloy 23-9.

Weld solidification substructure boundaries were not readily apparent in any of the weld microstructures. Closer examination of the Ferralium Alloy 255 microstructure (Fig. 4) did indicate that the intragranular austenite may precipitate along prior substructure (cellular or dendritic) boundaries. As mentioned previously, during solidification as primary ferrite, nickel partitions to the solidification boundaries (Refs. 20, 22, 23). Assuming diffusion is insufficient to eliminate the local nickel enrichment, this boundary will become a preferential site for austenite precipitation during cooling through the austenite plus ferrite phase field (Fig. 2). As the Cr_{eq}/Ni_{eq} increases, diffusion is more pronounced, since the weld cools through a larger temperature range in the ferrite phase field before the austenite transformation begins. As a result, any evidence of prior solidification structure or tendency for intragranular austenite precipitation is severely reduced.

Varestraint Test Results

The results of mini-Varestraint tests for the four duplex alloys and two Type 304L alloys are summarized in Table 3. The best index of the relative fusion zone hot cracking susceptibility was provided by plotting the total crack length (TCL) on the specimen surface versus the augmented strain over the range from ½ to 5%, as illustrated in Fig. 5. Using this index, the Ferralium Alloy 255 proved to be the most susceptible to hot cracking of the duplex alloys over the entire range of augmented strain. At intermediate strain levels (2 and 3%), the hot cracking susceptibility of Ferralium Alloy 255 and Uddeholm NU744LN were essentially identical, but both exceeded that of the experimental alloys (21-9 and 23-7) and the Type 304L alloy with 4.5 FN. At the lowest levels of augmented strain (below 1.5%), all the alloys tested, with the exception of the fully austenitic Type 304L material, exhibited equivalent crack

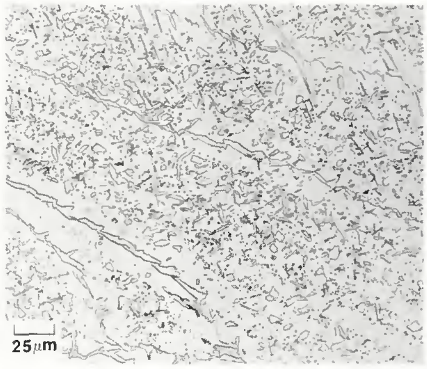

Fig. 4—Ferralium Alloy 255 fusion zone microstructure. Note the alignment of intragranular austenite along the solidification growth direction

Table 3—Summary of Mini-Varestraint Test Results

Material	% Strain	No. Cracks	TCL (mm)
Ferralium Alloy 255	1.0	2	0.41
	1.5	4	0.76
	2.1	13	3.00
	3.1	24	6.24
	5.0	40	10.44
Uddeholm NU744LN	1.0	4	0.34
	1.5	4	0.41
	2.1	16	2.42
	3.1	24	5.57
	5.0	31	6.31
Alloy 21-9	0.5	0	0
	1.0	0	0
	2.1	5	0.72
	3.1	21	3.58
	5.0	43	7.10
Alloy 23-7	0.5	0	0
	1.0	0	0
	2.1	15	1.18
	3.1	12	2.23
	5.0	35	5.98
Type 304L (FN 5)	0.5	0	0
	1.0	0	0
	2.1	5	0.47
	3.1	33	2.65
	5.0	46	5.55
Type 304L (FN 0)	0.5	6	1.73
	1.0	16	6.23
	2.1	21	8.92
	3.1	24	11.86

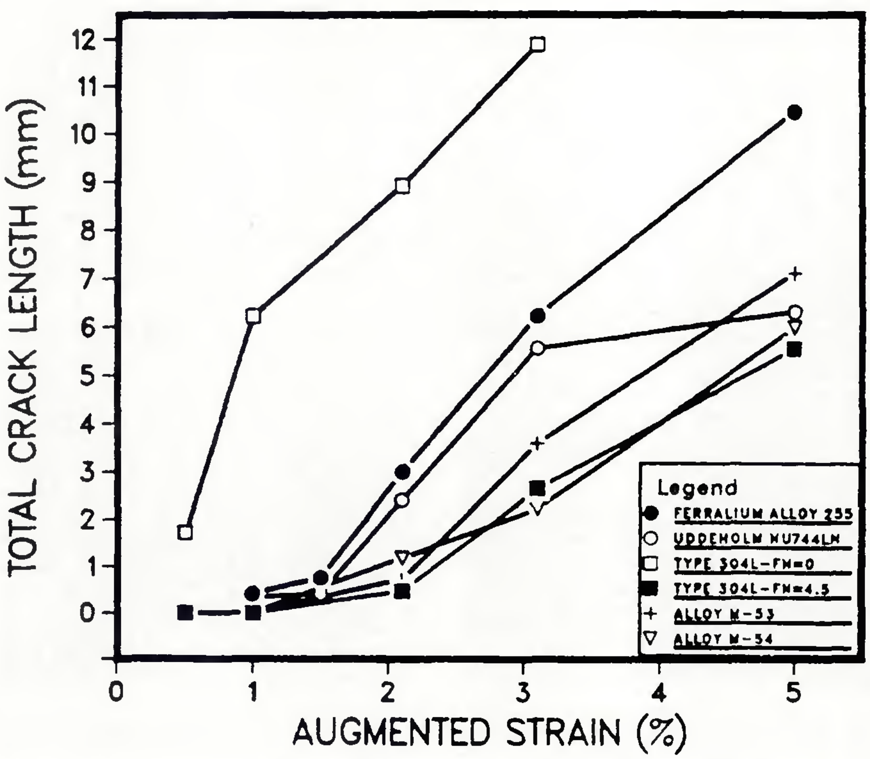

Fig. 5—Results of the mini-Varestraint test in terms of total crack length vs. augmented strain

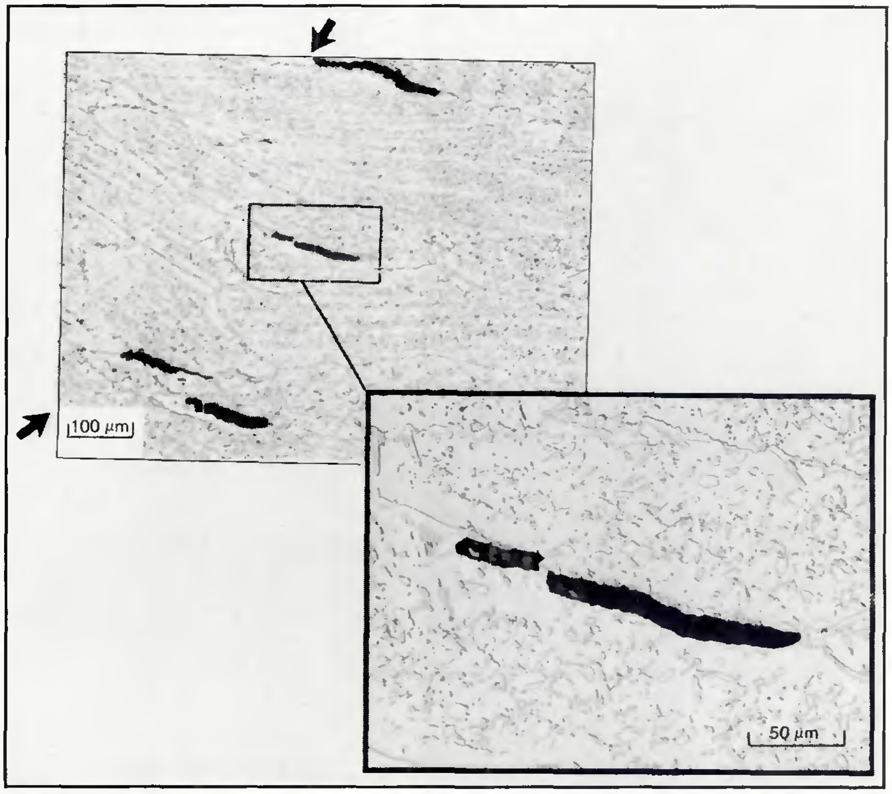

Fig. 6 — Fusion zone hot cracking in a Ferralium Alloy 255 Varestraint sample tested at 5% strain (top surface section). Arrows indicate the approximate location of the solid-liquid interface at the instant of testing

susceptibilities. None of the duplex alloys approached the high degree of crack susceptibility found in the fully austenitic Type 304L alloy.

The average length of hot cracks at a particular strain level may also be used as a measure of the degree of susceptibility to cracking and often provides an indication as to the relative magnitude of the embrittlement temperature range (Ref. 36). The average crack length (ACL) at 3.1% strain for the four duplex materials and the two 304L alloys is presented in Table 4. The ACL for the duplex materials is two to three times greater than that of the Type 304L alloy with FN 4.5, but is only one-third to one-half that of the fully austenitic Type 304L alloy. Assuming that the temperature gradient into the solid is nearly linear at temperatures just below the liquidus and relatively uniform for all the materials (welding parameters were identical), the embrittlement temperature range for fully ferritic or fully austenitic solidification would appear to be significantly greater than when austenite is a secondary solidification product, *i.e.*, Type 304L, FN 4.5.

Metallographic Analysis of Varestraint Samples

Metallographic examination of the duplex stainless steel Varestraint samples revealed that hot cracking in all four materials was associated with fusion zone grain boundaries. Partitioning of alloy and impurity elements is generally greater along these grain boundaries than at the subgrain boundaries (Refs. 7, 8, 22), and thus weld hot cracking is more prevalent at these sites[1].

The top surface of a Ferralium Alloy 255 Varestraint sample tested at 5% strain is shown in Fig. 6. The hot cracks were distributed around the periphery of the solid-liquid interface at the instant of applied strain. As noted, the cracks shown in Fig. 6 were located at grain boundaries in the Ferralium Alloy 255 microstructure. These boundaries were delineated by the continuous austenite networks.

At higher magnification (inset, Fig. 6), note that austenite side plates emanated from the crack boundaries. Since it is likely that solidification of Ferralium Alloy 255 occurred entirely as ferrite (no eutectic/peritectic reaction), this austenite formed during cooling from the solidification range. Thus, the hot crack shown in Fig. 6 initiated and propagated along ferrite-ferrite grain boundaries.

A transverse metallographic section from a Ferralium Alloy 255 Varestraint sample is shown in Fig. 7. This section was located such that the subsurface hot cracks which formed during the Varestraint test were revealed. The solidification growth direction was nearly vertical in Fig. 7. This growth orientation resulted in relatively straight grain boundaries, which facilitated crack propagation.

A metallographic section representative of the top surface of a Uddeholm NU744LN Varestraint sample is shown in Fig. 8. Again, note that hot cracking was restricted to the prior-ferrite grain boundaries, as delineated by the continuous austenite networks. Similar metallographic sections are presented for Alloy 21-9 and Alloy 23-7 in Fig. 9.

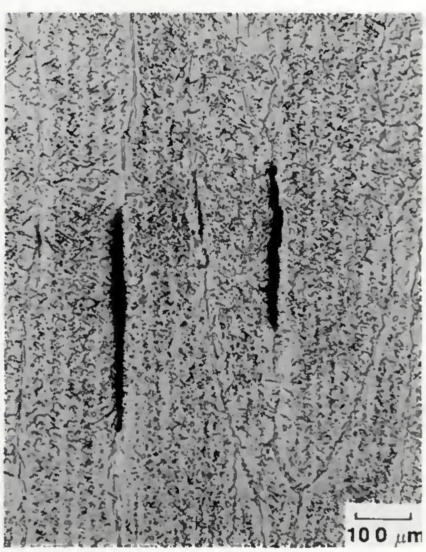

Fig. 7 — Transverse section of a Ferralium Alloy 255 Varestraint specimen tested at 3% strain. Note the straight grain boundaries along which cracks propagate

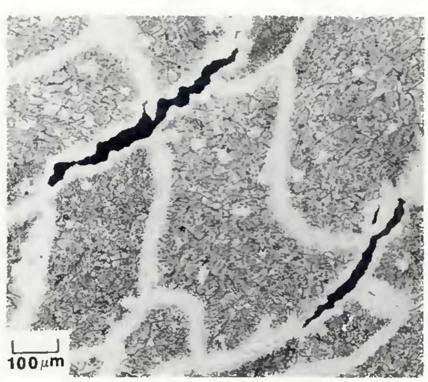

Fig. 8 — Fusion zone hot cracking in a Uddeholm NU744LN Varestraint specimen tested at 5% strain

1. Two types of grain boundaries may exist in the weld fusion zone. One type results from the impingement of solidification subgrains of different growth orientation and is delineated by both the growth orientation mismatch and elemental segregation. The other type results from migration of this boundary on cooling from the solidification temperature range. The former is the usual site for weld hot cracking and, unless otherwise specified, will be the type implied in this paper when discussing the weld fusion zone microstructure.

phology of the Type 304L alloys was also examined and is shown in Fig. 10. Hot cracks in the fully austenitic (FN 0) Type 304L Varestraint specimens were associated with relatively straight fusion zone grain boundaries (Fig. 10A), similar to the morphology exhibited by the duplex alloys (Figs. 6–9). In contrast, hot cracks in the Type 304L alloy which exhibited FN 4.5 were extremely short and could not be associated with a distinct fusion zone grain boundary (Fig. 10B).

Heat-affected zone cracking was not observed in either the duplex alloys or the Type 304L alloy with FN 4.5, even at the highest level of restraint. In contrast, heat-affected zone cracking was routinely observed in the fully austenitic Type 304L alloy. These HAZ cracks were usually continuous across the fusion line, suggesting that the cracks initiated in the fusion zone and propagated into the heat-affected zone.

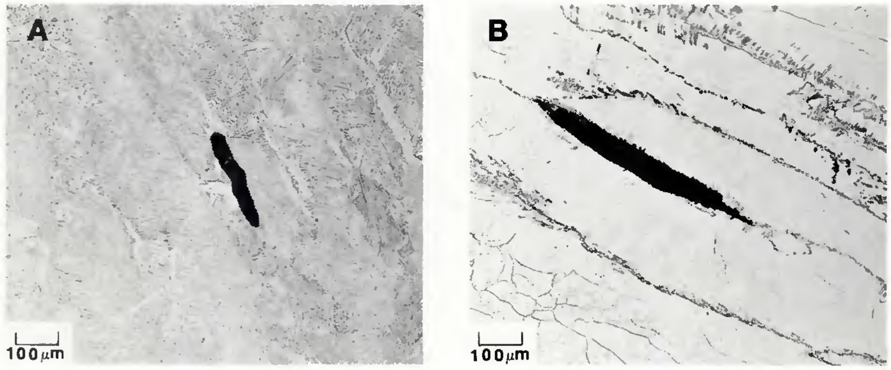

Fig. 9 — Fusion zone hot cracking in experimental duplex stainless steel Varestraint specimens tested at 5% strain. A — Alloy 21-9; B — Alloy 23-7

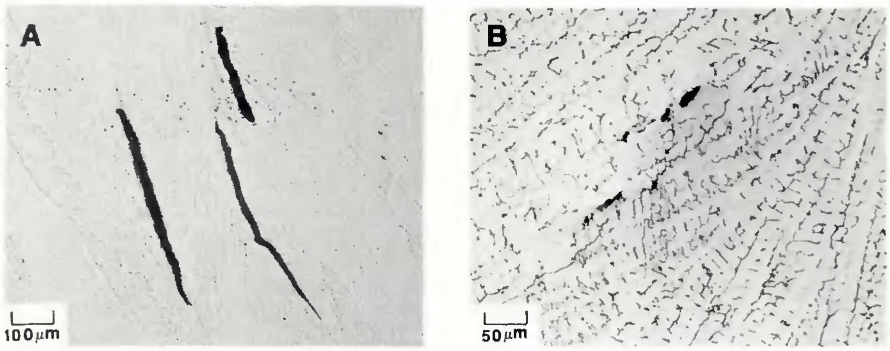

Fig. 10 — Fusion zone hot cracking in Type 304L Varestraint specimens tested at 5% strain. A — FN 0; B — FN 4.5. Note difference in magnification

Fractography

Figure 11A, which illustrates a hot crack fracture surface in Ferralium Alloy 255, clearly reveals the fine protrusions which correspond to cellular-dendrite primary and secondary arms and which are commonly associated with a solidification-related fracture surface. An examination of this fracture surface at increased magnification also revealed a transition in this fracture surface morphology from a relatively smooth, intergranular appearance on the surface of the crack most distant from the solid-liquid interface to an increasingly dendritic structure nearer this interface (Figs. 11B and 11C). The generally "wavy" appearance of this surface at high magnification confirmed that the crack was completely solidification-related, and that crack extension by a solid-state "ductility dip" process was unlikely. Fracture in the Uddeholm NU744LN and experimental duplex stainless steels appeared very similar to that observed in the Ferralium 255. As indicated in Figs. 12A and 12B, there was strong evidence of the fracture of dendrites which may have acted as bridges separating the areas of low-melting liquid. However, the characterization of matching opposite sides in order to confirm this possibility was not conducted.

Microprobe and Auger Analysis

Weld hot cracking is usually associated with liquid films which persist along fusion zone grain boundaries, thus extending the effective solidification temperature range of the weld metal. The analysis of the remnants of these liquid films is often useful in determining the nature of the cracking. Since these films tend to be extremely thin, electron optics techniques are usually employed to determine their nature. The electron microprobe is particularly well suited for analyzing bulk samples.

A region along the tip of a hot crack in a Ferralium Alloy 255 sample is shown in Fig. 13. Analysis at several points along the crack path, as indicated in Fig. 13, revealed an increase in molybdenum, copper, nickel, and phosphorus relative

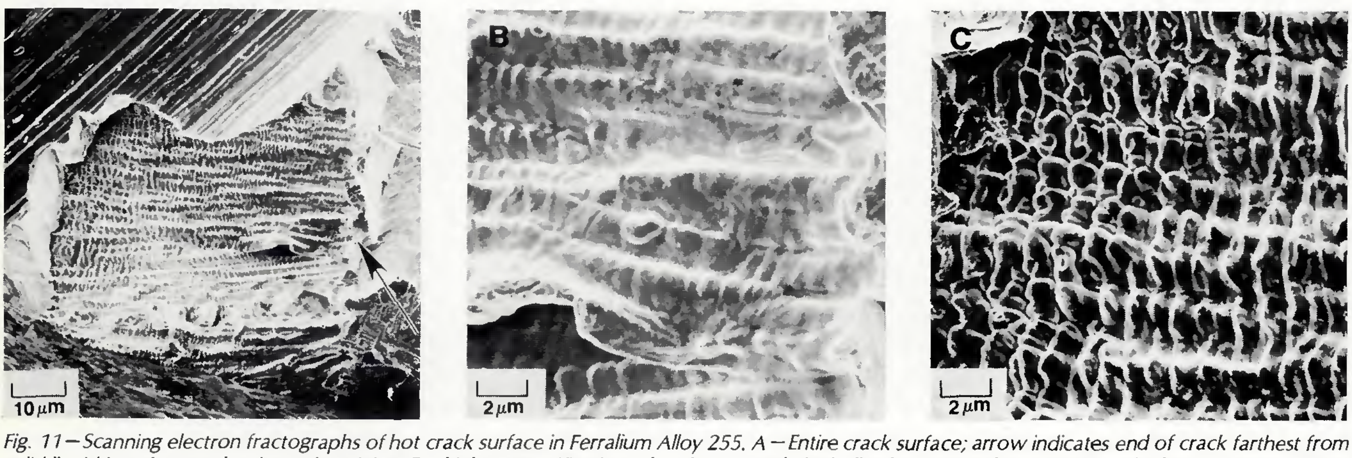

Fig. 11 — Scanning electron fractographs of hot crack surface in Ferralium Alloy 255. A — Entire crack surface; arrow indicates end of crack farthest from solid-liquid interface at the time of straining; B — higher magnification of A showing relatively flat fracture surface in regions farthest from solid-liquid interface; C — higher magnification of A showing more dendritic-appearing fracture surface nearer the solid-liquid interface

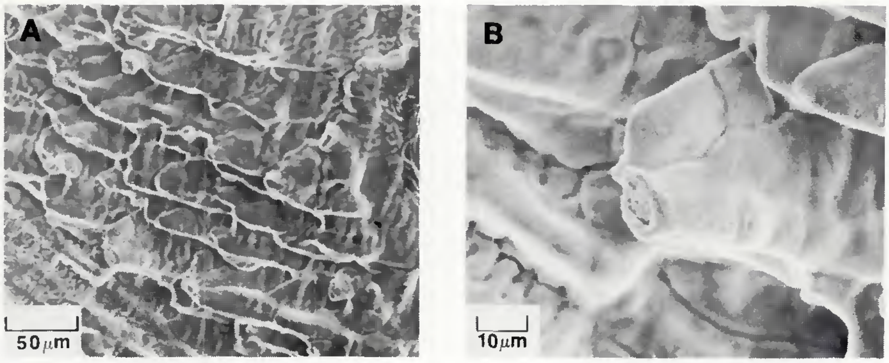

Fig. 12 — Scanning electron fractographs of hot crack surface in Uddeholm NU744LN. A — Dendritic-appearing fracture surface; B — higher magnification of A showing apparent "fractured" dendrite

to the bulk composition. The analysis was confounded somewhat by the austenite transformation which occurred along the boundary subsequent to the formation of the hot crack. Partitioning of austenite-forming elements (primarily Ni) to the fusion zone grain boundaries during primary ferrite solidification promoted the formation of austenite at these sites, but it was unclear to what degree diffusion following solidification modified the boundary composition. For instance, under equilibrium conditions, both nickel and copper would tend to diffuse to the austenite during the ferrite-austenite transformation. During rapid cooling following solidification, however, diffusion of these elements would be more restricted.

Auger surface analysis is also useful in determining the composition of thin films on hot crack fracture surfaces. Since cracks propagate along a liquid grain boundary film, the surface of these cracks will reflect the composition of the liquid. Again, the analysis was confounded both by the solid-state transformation that occurred along the boundary during cooling and by high-temperature diffusion. An Auger compositional profile to an approximate 100-nm depth on the surface of a hot crack in a Ferralium Varestraint specimen is shown in Fig. 14.

The depth profile was performed in a region of the fracture surface which exhibited the dendritic morphology typical of solidification cracks. Note that molybdenum, nickel, copper, silicon, nitrogen, and sulfur are present in appreciable concentrations in the near-surface layer. These results corroborate the electron microprobe results and indicate that higher levels of molybdenum and sulfur may be associated with the grain boundary film than were apparent from the microprobe analysis. In contrast to the microprobe results, phosphorus was not detected on the fracture surface by the SAM. This discrepancy may be due to either insufficient data or to the precipitation of discrete phosphides along the solidification boundary, which may have escaped detection by the highly localized Auger technique.

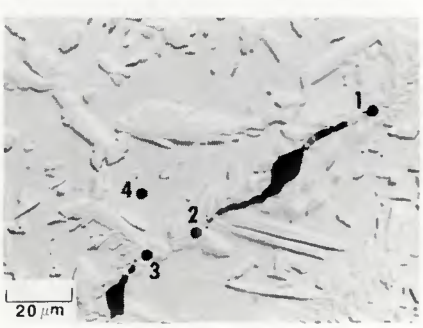

Fig. 13 — Electron microprobe analysis results near the crack tip in a Ferralium Alloy 255 Varestraint specimen

Discussion

Evaluation of Varestraint Test Results

Weld hot cracking is the product of a crack-susceptible microstructure and weld restraint during solidification. In theory, fusion zone microstructures in all but pure materials (or alloys which solidify at an invariant point, such as a eutectic) may be susceptible to cracking during the final stages of solidification. In practice, the relative susceptibility of welds to hot cracking is measured by the amount of strain that the microstructure can accommodate during solidification. Weld microstructures which can accommodate large imposed strains during solidification are resistant to hot cracking, while those which fail at low levels of restraint are judged susceptible. The Varestraint test is a useful tool for both determining the degree of strain accommodation in a particular microstructure and comparing that behavior with alternate microstructures.

In this investigation, the Varestraint test results have shown that the commercial duplex stainless steels (Ferralium Alloy 255 and Uddeholm NU744LN) are more susceptible to weld solidification cracking than a Type 304L alloy which solidified as ferrite and exhibited a fusion zone microstructure with FN 4.5. Conversely, these commercial duplex stainless steels were more resistant to cracking than a Type 304L alloy which solidified as austenite and was fully austenitic (FN 0) at room temperature. The cracking susceptibility of the experimental duplex alloys (23-7 and 21-9) approached that of the Type 304L alloy with FN 4.5.

Field experience with commercial duplex stainless steels (Refs. 28–30) suggests that these materials are relatively immune to weld hot cracking and compare favorably with 300-series stainless steels which produce a weld microstructure with FN 3–10. The apparent discrepancy between field experience and the Varestraint results (Fig. 5) may be explained by considering the level of solidification-induced strain to which the field welds are subjected. In Fig. 5, note that at augmented strain levels below approximately 2%, the duplex stainless steels exhibit the same resistance to cracking as the Type 304L alloy with FN 4.5. Varestraint tests at restraint levels below 2% are probably more representative of the actual welding practice using conventional processes (SMAW, GTAW, GMAW). As a result, the satisfactory weld cracking resistance of the duplex stainless steels which has been reported is, in fact, predicted by the Varestraint test.

The fully austenitic Type 304L alloy exhibited a significant increase in cracking susceptibility relative to the duplex stainless steels at all levels of augmented strain. This large difference in cracking susceptibility is in general agreement with service experience using fully austenitic stainless steel weld metals.

At higher levels of weld restraint (> 2%), the susceptibility of the duplex stainless steels to weld hot cracking was found to increase relative to Type 304L with FN 4.5. Specifically, at 3.1% strain (Fig. 5) the cracking susceptibility of the duplex alloys was approximately midway between that exhibited by the two Type 304L variants. This relative increase in susceptibility at higher strain levels suggests that the duplex stainless steels may experience weld cracking problems in applications where the weld restraint is high (for example, high depth-to-width restrained joints).

The difference in cracking susceptibility at higher strain levels may result from several factors, including the possibility that at lower strains the solidification boundary strength may be sufficient to resist separation, despite the presence of low-melting liquid at these boundaries. Above some critical strain level (1.5–2%), the boundary strength may be insufficient to prevent separation, resulting in the formation of a hot crack.

Despite the similarity in solidification behavior, the experimental duplex alloys are, in general, less susceptible to weld hot cracking than the commercial alloys. Differences in solidification crack susceptibility among similar alloys are often the result of slight variations in chemical composition, particularly with respect to impurity content. Table 1 shows that the level of sulfur and phosphorus in the experimental alloys was higher than that in the commercial alloys. Thus, the increase in cracking susceptibility due to higher impurity levels is not possible.

Note that both copper and molybdenum are present in the Ferralium (1.7Cu, 3.1Mo) and Uddeholm (0.2Cu, 2.4Mo) alloys but absent in the experimental alloys. Electron microprobe and Auger analysis of solidification grain boundaries (Fig. 13) and hot crack fracture surfaces (Fig. 14) of these alloys revealed an increase in both of these elements at these locations. Other elemental segregation (Ni, Mn, Si, P, S) to the solidification grain boundaries was similar among the duplex alloys and thus does not explain the difference in cracking susceptibility.

Copper and molybdenum both depress the melting point of Fe-base alloys (Refs. 37, 38). As a result, significant localized segregation of these elements to solidification grain and subgrain boundaries would likely reduce the solidification temperature relative to the surrounding weld microstructure and expand the effective solidification range of the weld. Unfortunately, it is difficult to predict the effect of individual alloying or impurity elements on hot cracking susceptibility in multicomponent systems from simple equilibrium binary systems. Synergistic interactions with other alloying (Ni, Mn, Cr, Si, C, N) or impurity elements (S and P) may promote the formation of liquid films along fusion zone boundaries, which would not be predicted by consideration of simple binary reactions. These same synergisms may enhance the wetting characteristics of the liquid along ferrite grain boundaries and further increase the cracking susceptibility.

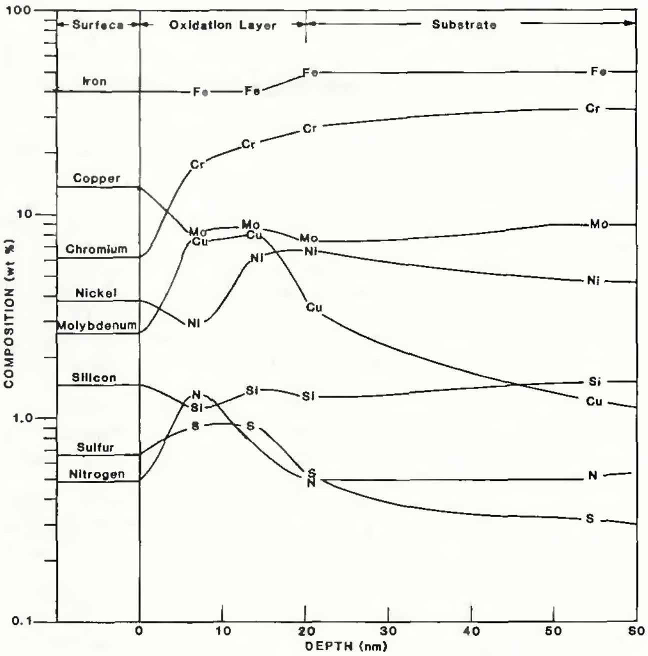

Fig. 14 — Auger depth profile showing the concentration of elements on a Ferralium Alloy 255 hot crack surface. Carbon and oxygen were present as a 20-nm-thick contamination layer but have been omitted for clarity

Hot Crack Morphology

Hot crack surfaces generally exhibit fine protuberances associated with primary and secondary cellular-dendrite arms. In the present study, the careful examination of hot crack surfaces for the duplex stainless steels also revealed a columnar, microscopically flat region, and a gradual transition from this flat fracture near the rear portion of the hot crack (that farthest from the solid-liquid interface at the time of straining) to increasingly dendritic fracture near the front of the crack. Similar transitions in hot crack surface topography have been reported previously in stainless steels which solidify to either fully ferritic or fully austenitic structures (Refs. 39-41), and have been attributed to a decrease in the quantity of residual liquids at interdendritic regions with decreasing temperature. Little tendency for the flat columnar fracture surface has been reported for hot cracks in welds which exhibit coupled ferrite/austenite solidification along fusion zone grain and subgrain boundaries and which contain a small amount of ferrite (FN 3-10) in the room temperature microstructure (Ref. 39). These results are consistent with the fractographic analysis of the FN 4.5 Type 304L alloy evaluated in the present investigation.

In order to understand the origin of the flat fracture on the surface of the weld hot cracks in the duplex alloys, and determine how this morphology relates to cracking susceptibility, it is necessary to define the boundary along which the fracture occurs. The fusion zone grain boundaries along which hot cracking is most prevalent originate by the impingement of cellular dendrites of different growth orientation during the final stages of solidification. Microscopically, this boundary would be expected to be very irregular during the final stages of solidification, and thus would tend to migrate following solidification in an effort to minimize the total grain boundary area. Evidence of such grain boundary migration is often visible in the room temperature microstructure as a difference between the actual grain boundary and the original solidification boundary, as delineated by the presence of residual, segregated alloying elements.

The examination of flat fracture surfaces in the duplex alloys studied in this investigation showed columnar-shaped, smooth fracture surfaces comparable to those commonly observed for intergranular corrosion or mechanical fracture in the weld fusion zone, suggesting that this region is associated with crack propagation along a migrated grain boundary. This possibility is supported by Matsuda and Nakagawa (Ref. 39), who suggest that the flat fracture originates from grain boundary migration among residual liquids in the low-temperature crack region, and by Dixon and Phillips (Ref. 41), who relate flat fracture to the formation of grain boundaries during the final stages of solidification. Unfortunately, details of these grain boundary phenomena during the final stages of solidification have not been reported. Although the present investigation did not identify the specific origin of the flat fracture region, several potential explanations can be offered. These include:

1. Grain boundary migration and straightening while liquid is still present in a continuous or semi-continuous distribution.

2. Liquid penetration under a state of stress of a solidified and migrated grain boundary (analogous to liquid metal embrittlement).

3. The occurrence of solid-state "ductility-dip" cracking.

As noted above, Type 304L stainless steels exhibiting FN 3-15 display an exclusively dendritic crack surface (Ref. 39). Matsuda and Nakagawa (Ref. 39) suggest that this absence of flat fracture is related to the peritectic/eutectic reaction experienced during solidification of most Type 304 stainless steels, which prevents the grain boundary from migrating and straightening at near-solidus temperatures. The concept of such grain boundary irregularity or tortuosity reducing hot cracking in austenitic stainless steels was originally proposed by Matsuda (Ref. 36) and later by Brooks (Ref. 23) to explain the cracking resistance of the low FN stainless steel welds. In weldments which solidify completely to austenite or ferrite, this grain boundary motion is not restricted, which results in a less tortuous boundary and a greater cracking sensitivity. Correlations of quantitative cracking results with fractography results discussed above for the present investigation support this proposed grain boundary tortuosity effect on hot cracking susceptibility.

Conclusions

1. Varestraint test results show the commercial duplex stainless steels, Ferralium Alloy 255 and Uddeholm NU744LN, to be more susceptible to fusion zone hot cracking than Fe-Cr-Ni experimental duplex alloys which exhibit similar solidification behavior.

2. Varestraint test results show that the commercial duplex stainless steels are more susceptible to cracking at high levels of augmented strain than a FN 4.5 Type 304L stainless steel, but less susceptible than a FN 0 Type 304L stainless steel over the entire range of strain.

3. Fusion zone hot cracking in the duplex stainless steels occurred exclusively along ferrite grain boundaries. HAZ cracking in the duplex alloys was not observed in the duplex or FN 4.5 Type 304L stainless steels, although it was present in the FN 0 Type 304L stainless steel.

4. Optical metallography in concert with electron microprobe and Auger analysis suggest that the greater cracking susceptibility of the commercial duplex stainless steels resulted from the likely formation of a complex, low-melting liquid film enriched in copper and phosphorus.

5. Fractographic examination of the fracture surfaces showed a transition from dendritic to flat fracture exclusively in the single-phase-solidifying duplex stainless steels. The existence of this flat fracture has been related to the greater cracking susceptibility of these alloys versus the FN 4.5 Type 304L stainless steel, which exhibited only dendritic fracture.

Acknowledgments

The authors are grateful to Andy Gardea, Clarence Karfs, Miles Clift and Dave Ruddle, all from Sandia National Laboratories, Livermore, Calif., whose willing assistance and technical skills were invaluable during the course of this investigation. This work was supported in part by the U.S. Department of Energy (DOE) under Contract No. DE-AC04-75DP00789.

References

1. Solomon, H. D., and Devine, T. M. 1983. A tale of two phases. *Conf. Proc. Duplex Stainless Steels,* ASM, pp. 693-756.

2. DeBold, T. A., Martin, J. W., and Tverberg, J. C. 1983. Duplex stainless offers strength and corrosion resistance. *Ibid.,* pp. 169-189.

3. Poznansky, A., Nalbone, C. S., and Crawford, J. D. 1983. The corrosion resistance of 25Cr-3.5Mo-6Ni and 25Cr-4.5Mo-6Ni cast duplex stainless steels. *Ibid.,* pp. 431-444.

4. Honeycombe, J., and Gooch, T. G. 1977. Intergranular attack in welded stress-corrosion resistant stainless steels. *Welding Journal* 56(11):339-s to 353-s.

5. Tynell, M. 1983. Applicability range for a high strength duplex stainless steel in deep sour oil and gas wells. *Conf. Proc. Duplex Stainless Steels,* ASM, pp. 283-292.

6. Miyuki, H., Kudo, T., Koso, M., Miura, M., and Moroishi, T. 1983. 25%Cr containing duplex phase stainless steel for hot sea water applications. *Ibid.,* pp. 95-112.

7. Savage, W. F., Lundin, C. D., and Aronson, A. H. 1965. Weld metal solidification mechanics. *Welding Journal* 44(4):175-s to 181-s.

8. Savage, W. F., Nippes, E. F., and Miller, T. W. 1976. Microsegregation in 70Cu-30Ni weld metal. *Welding Journal* 55(6):165-s to 173-s.

9. Borland, J. C. 1960. Generalized theory of super-solidus cracking in welds and castings. *Brit. Weld. Jour.* 7(8):508-512.

10. Apblett, W. R., and Pellini, W. S. 1954. Factors which influence weld hot cracking. *Welding Journal* 33(2):83-s to 90-s.

11. Medovar, B. I. 1954. On the nature of weld cracking. *Avtom. Svarka* 7(4):12-18.

12. Borland, J. C. 1960. Hot cracking in welds. *Brit. Weld. Jour.* 7(9):558-559.

13. Scherer, R., Riedrich, G., and Hougardy, H. 1941. Welding Rod, U.S. Patent 2,240,672.

14. Borland, J. C., and Younger, R. N. 1960. Some aspects of cracking in welded Cr-Ni austenitic steels. *Brit. Weld. Jour.* (1):22-59.

15. Hull, F. C. 1967. Effect of delta ferrite on the hot cracking of stainless steel. *Welding Journal* 46(9):399-s to 409-s.

16. Fredriks, H., and Vander Toorn, L. J. 1968. Hot cracking in austenitic stainless steel weld deposits. *Brit. Weld. Jour.* (4):178-182.

17. Masumoto, I., Tamaki, K., and Kutsuna, M. 1972. Hot cracking of austenitic weld metal. *Trans. JWS* 41(11):1306-1341.

18. Arata, Y., Matsuda, F., and Saruwatari, S. 1974. Varestraint test for solidification crack susceptibility in weld metal of austenitic stainless steels. *Trans. JWRI* 3(1):79-88.

19. Lundin, C. D., DeLong, W. T., and Spond, D. F. 1975. Ferrite-fissuring relationship in austenitic stainless steel weld metals. *Welding Journal* 54(8):241-s to 246-s.

20. Suutala, N., Takalo, T., and Moisio, T. 1980. Ferritic-austenitic solidification mode in austenitic stainless steel welds. *Met. Trans.* 11A(5):717-725.

21. Matsuda, F., Nakagawa, H., Uehara, T., Katayama, S., and Arata, Y. 1979. A new explanation for the role of delta-ferrite in improving weld solidification crack susceptibility in austenitic stainless steel. *Trans. JWRI* 8(1):105-112.

22. Lippold, J. C., and Savage, W. F. 1982. Solidification of austenitic stainless steel weldments: part 3—the effect of solidification behavior on hot cracking susceptibility. *Welding Journal* 61(12):388-s to 396-s.

23. Brooks, J. A., Thompson, A. W., and Williams, J. C. 1984. A fundamental study of the beneficial effect of delta ferrite in reducing weld cracking. *Welding Journal* 63(3):71-s to 83-s.

24. Ogawa, T., and Tsunetomi, E. 1982. Hot cracking susceptibility of austenitic stainless steels. *Welding Journal* 61(3):82-s to 93-s.

25. Arata, Y., Matsuda, F., and Katayama, S. 1977. Solidification crack susceptibility in weld metals of fully austenitic stainless steels (report II). *Trans. JWRI* 6(1):105-116.

26. Takalo, T., Suutala, N., and Moisio, T. 1979. Austenitic solidification mode in austenitic stainless steel welds. *Met. Trans.* 10A (8):1173-1181.

27. Suutala, N., Takalo, T., and Moisio, T. 1979. Single-phase ferritic solidification in austenitic-ferritic stainless steel welds. *Met. Trans.* 10A(8):1183-1190.

28. Blumfield, D., Clark, G. A., and Guha, P. 1981. Welding duplex austenitic-ferritic stainless steel weldments. *Metal Construction* 13(5):269-273.

29. Gooch, T. G. 1983. Weldability of duplex ferritic-austenitic stainless steels. *Conf. Proc. Duplex Stainless Steels,* ASM, pp. 573-602.

30. Flasche, L. H. 1983. Weldability of Ferralium Alloy 255. *Ibid.,* pp. 553-572.

31. Lundin, C. D., Lingenfelter, A. C., Grotke, G. E., Lessmann, G. G., and Matthews, S. J. 1982. The Varestraint test. *Weld. Res. Council Bulletin,* No. 280.

32. Berry, W. E. 1967. Procedures for quantitative removal of oxide scales formed in high temperature water and steam. *Materials Protection* 6(7):69.

33. Lippold, J. C., and Savage, W. F. 1979. Solidification of austenitic stainless steel weldments, part 1—a proposed mechanism. *Welding Journal* 58(12):361-s to 374-s.

34. Kotecki, D. J. 1982. Extension of the WRC ferrite number system. *Welding Journal* 61(11):352-s to 361-s.

35. Greulich, F. A. 1985. Unpublished research performed at Sandia National Laboratories, Livermore, Calif.

36. Matsuda, F., Nakagawa, H., Uehara, T., Katayama, S., and Arata, Y. 1979. A new explanation for the role of delta ferrite in improving the weld solidification crack susceptibility in austenitic stainless steel. *Trans. JWRI* 8(1).

37. Hellawell, A., and Hume-Rothery, W. 1957. *Phil. Trans. Royal Society of London,* Ser. A, 249:417-459.

38. Sinha, A. K., Buckley, R. A., and Hume-Rothery, W. 1967. *J. Iron and Steel Inst.* 205:191-195.

39. Matsuda, F., and Nakagawa, H. 1979. Fractographic features and classification of weld solidification cracks. *Trans. JWRI* 8(1).

40. Dixon, B. F., and Phillips, R. H. Cracking in the trans-Varestraint test, part 3—fractography. *Metal Construction* (4):232-237.

41. Katayama, S., Fujimoto, T., and Matsunawa, A. 1985. Correlation among solidification process, microstructure, microsegregation and solidification cracking susceptibility in stainless steel weld metals. *Trans. JWRI* 14(1).